Future Cities and Environment
ISSN 2363-9075 Volume 12 (2026)

https://doi.org/10.70917/fce-2026-011
Article

Low-Cost Solutions for Concrete Enhancement: Assessing Steel Clamp Efficacy

Kittipoom Rodsin [1], Chichaya Boonmee [2,*] Ali Ejaz [3], Burachat Chatveera [4], Gritsada Sua-iam [5], Tahir Mehmood [6], Qudeer Hussain [1], Preeda Chaimahawan [7,*], Chisanuphong Suthumma [8,*],

[1] Center of Excellence in Structural Dynamics and Urban Management, Department of Civil and Environmental Engineering Technology, College of Industrial Technology, King Mongkut's University of Technology North Bangkok, Thailand; kittipoom.r@cit.kmutnb.ac.th (K.R.); ebbadat@hotmail.com (Q.H.)
[2] Department of Teacher Training in Civil Engineering, Faculty of Technical Education, King Mongkut's University of Technology North Bangkok, Bangkok 10800, Thailand
[3] National Institute of Transportation, National University of Sciences and Technology (NUST), Islamabad 44000, Pakistan; enggaliejax@gmail.com
[4] Department of Civil Engineering, Faculty of Engineering, Thammasat University (Rangsit campus), Pathum Thani 12121, Thailand; cburacha@engr.tu.ac.th
[5] Department of Civil Engineering, Faculty of Engineering, Rajamangala University of Technology Phra Nakhon, Bangkok, 10800, Thailand; gritsada.s@rmutp.ac.th
[6] Architecture and Civil Engineering Department, Sultan Qaboos University, Muscat 123 OMAN, t.mehmood@squ.edu.om
[7] School of Engineering, University of Phayao, Phayao 56000 , Thailand
[8] Department of Civil Engineering, Faculty of Engineering at Kamphaeng Saen, Kasetsart University, Nakhon Pathom 73140, Thailand
* Correspondence authors: chichaya.b@fte.kmutnb.ac.th (C.B.); preeda.ch@up.ac.th (P.C.); chisanuphong.s@ku.th (C.S.)

Abstract: This study evaluates the effectiveness of steel clamps as a low-cost passive confinement system for reinforced concrete (RC) under axial compression. Cylindrical RC specimens with different unconfined strengths, reinforcement types, and numbers of steel clamps (3, 5, and 11) were experimentally tested to investigate their influence on failure modes, compressive strength, strain capacity, and energy dissipation. The results show that steel clamp confinement significantly delayed cracking, improved ductility, and enhanced compressive performance. Peak compressive strength increased by up to 77%, while strain at peak strength and ultimate strain improved by up to 268% and 900%, respectively. Energy dissipation increased by nearly 2000% in highly confined specimens. Based on the experimental data, nonlinear regression-based expressions were developed to predict peak strength, peak strain, and post-peak degradation behavior, enabling accurate simulation of the full stress–strain response. The proposed analytical model follows the ACI 440 formulation style and provides a practical design-oriented tool for applying steel clamp confinement in RC elements.

Keywords: reinforced concrete; steel clamps; passive confinement; compressive response; analytical modeling

1. Introduction

Aging and exposure to harsh environments are major causes of deterioration in reinforced concrete (RC) structures. This damage often appears as concrete cracking, steel corrosion, and deformation in members, all of which reduce the structure's functioning and safety. As a result, practical and reliable strengthening methods are needed to restore RC structures (Ejaz et al. 2022). In many cases, structures also require increased load-carrying capacity to support added loads ascribed to modifications in use or extensions to existing buildings (Park et al. 2008).

Confinement systems play a crucial role in improving the structural performance of RC members, particularly under axial and seismic loading. By restraining lateral expansion of concrete, confinement enhances compressive strength, ductility, and energy dissipation capacity, while delaying brittle failure (Saingam et al. 2025). These improvements are especially important in critical regions such as plastic hinge zones, bridge piers, and building columns subjected to earthquake, impact, or overload conditions (Gu et al. 2012). Confinement is widely employed in the rehabilitation of aging infrastructure, seismic retrofitting of deficient columns, upgrading of load-carrying capacity, and strengthening of members affected by material deterioration or design deficiencies. Both internal reinforcement and external jackets or wraps are commonly used to achieve confinement, depending on structural requirements, construction constraints, and economic considerations. Therefore, developing efficient, economical, and easy-to-apply confinement techniques remains a key objective in modern structural strengthening practice.

Conventional methods for strengthening deficient RC members typically involve externally wrapping the expected plastic hinge regions with concrete jackets (Chang et al. 2014; Vandoros and Dritsos 2008) or steel jackets (Aboutaha et al. 1996; Chai et al. 1991; Daudey and Filiatrault 2011; Lehman et al. 2001; Priestley and Seible 1995) However, these techniques are both labor-intensive and time-consuming (Raza et al. 2019; Salmaninezhad and Jazayeri Moghaddas 2021). Concrete jacketing increases the member size and adds significant weight to the structure, while steel jacketing is difficult to handle and is susceptible to corrosion on the inner surfaces (Askar et al. 2022). These enlarged sections and added weight can also change the stiffness of the structure, which may affect its overall behavior (Juntanalikit et al. 2016; Raza et al. 2019). In recent times, fiber-reinforced polymers (FRPs) have acquired wide fame for strengthening structural members (Gao et al. 2019). Their strength-to-weight ratio is much greater than that of conventional methods using steel or RC jackets, which makes FRPs a lighter and more efficient option (Haroun and Elsanadedy 2005). They also provide excellent resistance to corrosion (Wang et al. 2018). Because of these advantages, FRPs have been used in many strengthening applications, including flexural (Attari et al. 2012; Dong 2011; Erfan et al. 2021; Khalid Ali et al. 2022; del Rey Castillo et al. 2018), shear (Baggio et al. 2014; Chen and Teng 2003; Farghaly and Benmokrane 2013; Song et al. 2023), lap splices (Bournas and Triantafillou 2011; Bousias et al. 2004; ElGawady et al. 2009; Ghosh and Sheikh 2007; Harries et al. 2006), and compression strengthening (Jamatia and Deb et al. 2017; Jiang et al. 2020; Rousakis et al. 2007; Zeng et al. 2017). Experimental and numerical works consistently show that FRP confinement greatly enhances both the strength and ductility of concrete under compression. Numerous stress-strain expressions for FRP-confined concrete have been proposed for circular and non-circular shapes (Lim and Ozbakkaloglu et al. 2014; Ozbakkaloglu et al. 2013), leading to a better knowledge of its compressive response.

(Shaw and Andrawes 2017) performed single-point loading tests on three scaled down prestressed concrete (PC) beams that were first failed and then externally confined with carbon fiber reinforced polymer (CFRP) and glass fiber reinforced polymer (GFRP) wraps. Their findings showed that externally wrapped FRP for shear could restore and also surpass the original shear strength of the undamaged beams. (Jiang et al. 2019) conducted experiments on FRP-confined RC columns with varying bonding situations among FRP and concrete. They concluded that while bonding changes do not notably impact the overall response of the columns, slip at the interface can negatively influence the length of the plastic hinge zone.(Gao et al. 2024) improved the compressive performance of seawater sea-sand concrete by employing FRP confinement. (Saljoughian and Mostofinejad 2016) proposed a novel corner strip-batten method for FRP to enhance the compressive response of RC columns under eccentric loading. Synthetic FRP composites such as CFRP, GFRP, and AFRP are widely used for strengthening RC structures. However, several practical, economic, and environmental issues limit their broader adoption. A primary concern is their high material and installation cost, which can be several times greater than traditional methods, making them unsuitable for small-scale or low-budget projects (Saingam et al. 2024a; Yooprasertchai et al. 2023a). The production of synthetic FRPs is also energy-intensive, relying heavily on petroleum-based polymers and high-temperature manufacturing processes, which contribute to a significant carbon footprint compared to natural fiber composites (Faruk et al. 2012). Another challenge involves health and safety risks during fabrication and application. The resins, hardeners, and solvents used in FRP systems, particularly epoxy-based matrices, contain chemicals such as bisphenol-A epoxy, amine hardeners, and styrene, all of which may cause skin irritation, allergic contact dermatitis, and respiratory issues if proper protection is not used (Aljohani et al. 2025). Additionally, synthetic FRPs often exhibit poor performance at elevated temperatures, as matrix softening or degradation can occur at relatively low thresholds (60–120°C), reducing their effectiveness in fire conditions without additional insulation (Kodur et al. 2025). Disposal and recyclability also pose challenges; most synthetic FRPs are non-biodegradable, and recycling techniques such as thermal or chemical treatment are expensive, energy-demanding, and not widely available (Pickering 2006). These issues highlight the need for more sustainable, low-cost, and safer alternatives.

(Munir et al. 2021) used steel spiral confinement to improve the mechanical characteristics of recycled aggregate concrete. Their results showed that although the elastic modulus decreased with higher confinement levels, both the confined strength and its corresponding strain increased significantly. (Rodsin et al. 2022) later introduced a low-cost confinement technique using standard steel hose clamps to enhance the compressive behavior of recycled brick aggregate concrete (RBAC) in circular sections. They tested cylinders with two strength grades and applied 3, 5, and 11 clamps, reporting substantial gains in confined strength and a noticeable change in failure mode, with performance exceeding that of concrete made with natural aggregates. More recently, (Ejaz et al. 2025) applied steel clamps to strengthen square concrete specimens produced with either natural aggregates or RBA. They also proposed a unified model by combining their test data with the results reported by (Rodsin et al. 2022).

In the context of rapid urbanization and the development of future cities, a large portion of existing infrastructure is aging and requires efficient retrofit and upgrading strategies. Many RC structures in urban environments were designed according to outdated standards and exhibit insufficient strength, ductility, and resilience against extreme loading events. Cost-effective, easy-to-install strengthening techniques are therefore essential for extending service life and enhancing structural safety. The proposed steel clamp confinement system directly addresses these needs by providing a low-cost, scalable, and practical solution suitable for urban rehabilitation projects, temporary strengthening, and rapid retrofitting of critical infrastructure. Earlier works by (Rodsin et al. 2022) and (Ejaz et al. 2025) confirmed that steel clamp confinement is highly effective in enhancing the compressive performance of recycled or natural aggregate plain concrete. Although previous research has found that steel clamps can notably enhance the compressive behavior of plain concrete, its performance in RC remains unexplored. The presence of longitudinal and transverse reinforcement fundamentally alters stress distribution, crack propagation, and confinement interaction within RC members, meaning that results from plain concrete cannot be directly extended to structural elements containing steel bars. Reinforcement may either improve or hinder the effectiveness of steel clamps, and the combined confinement mechanism between internal steel reinforcement and external clamps is not yet understood. Since real structural members are almost always reinforced, it is essential to evaluate whether steel clamps can provide meaningful strength and ductility improvements under realistic conditions. Therefore, investigating steel clamp confinement for RC elements fills an important research gap and provides practical insights for developing a low-cost, easy-to-apply strengthening method suitable for actual structural applications. While external passive confinement using steel clamps has been previously demonstrated for plain concrete, this study uniquely extends the approach to reinforced concrete, addressing how internal longitudinal and transverse reinforcement alter the confinement mechanisms and resulting strength–ductility improvements

2. Materials and Methods

2.1. Specimen details and test matrix

Two main groups were formed in this work based on the type of longitudinal reinforcement, i.e., either plain or deformed bars of 9 mm diameter. All specimens were cylindrical in shape, having a diameter and length of 150 mm and 300 mm, respectively. Both groups were then split in two subgroups, depending on the unconfined concrete strength. That is, low and high strength level. It is important to note that the term “high” is relative to the lower strength and does not mean a “high strength” concrete. Both subgroups comprised four kinds of samples. One confined, serving as benchmark for the remaining three. Rest of three specimen types were confined with either three, five, or eleven steel clamps. To identify a specimen, three parts were used, as presented in Table 1. The first part represents unconfined strength, i.e., LS or HS for low or high strength, respectively. Then, the internal reinforcement was represented by either “P” or “D” corresponding to plain or deformed bars, respectively. Finally, the magnitude of steel clamps was represented by “3C”, “5C”, or “11C” corresponding to three, five or eleven clamps, respectively. Such that the name LS-D-5C shows a sample with low strength, featuring deformed longitudinal reinforcement, and confined with 5 steel clamps. Figure 1 shows the strengthening configuration, whereas Figure 2 depicts geometrical and structural details of specimens. Each specimen was reinforced with four longitudinal steel bars of 9 mm diameter arranged symmetrically along the cross-section. The bars were anchored using standard end hooks to prevent premature slip. No transverse reinforcement was provided in order to isolate the confinement effect of external steel clamps. The nominal yield strength and elastic modulus of the reinforcement were 420 MPa and 200 GPa, respectively. For each configuration, three identical specimens were fabricated and tested to ensure repeatability of results. The values reported in this study represent the average response of the tested specimens.

Table 1. Summary of experimental framework.

Group	Subgroup	ID	Unconfined Strength Type	Reinforcement Type	Steel Clamps
1	1A	LS-P-CON	LS	Plain	None
		LS-P-3C	LS	Plain	3
		LS-P-5C	LS	Plain	5
		LS-P-11C	LS	Plain	11
	1B	HS-P-CON	HS	Plain	None
		HS-P-3C	HS	Plain	3
		HS-P-5C	HS	Plain	5
		HS-P-11C	HS	Plain	11
2	2A	LS-D-CON	LS	Deformed	None
		LS-D-3C	LS	Deformed	3
		LS-D-5C	LS	Deformed	5
		LS-D-11C	LS	Deformed	11
	2B	HS-D-CON	HS	Deformed	None
		HS-D-3C	HS	Deformed	3
		HS-D-5C	HS	Deformed	5
		HS-D-11C	HS	Deformed	11

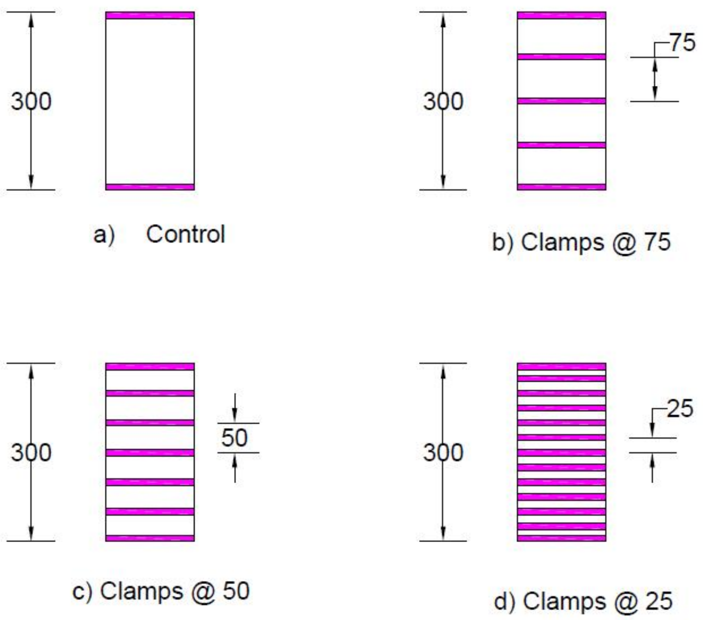

Figure 1. Configuration of steel clamps *(All units are in mm)*.

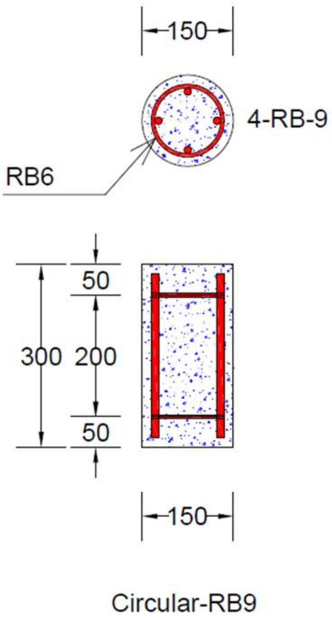

(a)

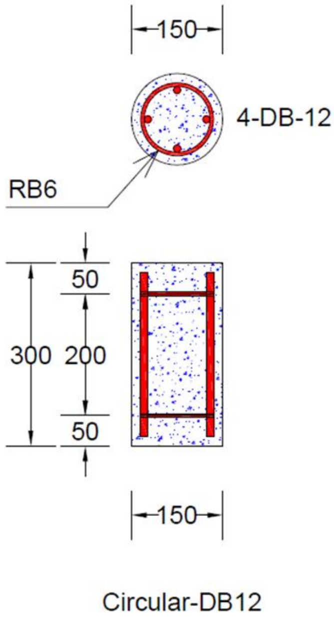

(b)

Figure 2. Geometrical and structural details of columns with (a) plain bars and (b) deformed bars. (All units in mm).

2.2. Material properties

Type I Portland cement conforming to relevant ASTM standards was used as the binder. Natural river sand with a fineness modulus of approximately 2.6 was employed as fine aggregate. The concrete mixes were proportioned to achieve target slump values of 70 mm for HS and 90 mm for LS. Coarse aggregates with sizes between 9.5 mm and 19.5 mm were included in the mixtures. The detailed mix proportions are provided in Table 2. Potable water was used for mixing and curing. All concrete batches were prepared using a mechanical mixer to ensure uniformity. Standard cylindrical specimens were cast alongside test specimens to determine the unconfined compressive strength at 28 days.

The tensile stress-strain behavior of the steel clamps was assessed following ASTM E8 (ASTM E8/E8M-21 rt al. 2021). Each clamp had a width of 10 mm and a thickness of 1.2 mm. The typical geometry and appearance of the clamps are shown in Figure 3(a), and their ductile stress–strain response is illustrated in Figure 3(b). To replicate actual strengthening conditions, the fastener was kept within the gage length during testing. These clamps were chosen because they are easy to apply and can be installed without the need for specialized tools. The tensile capacity of steel clamps was obtained to be 627 MPa.

Table 2. Mix design of concrete.

Concrete Type	Ingredients ($\mathbf{kg/m^3}$)				
	Cement	Sand	NCS	Brick Aggregates	Water
A	270	780	520	520	310
B	625	810	355	355	255

Steel clamp image here
(a)

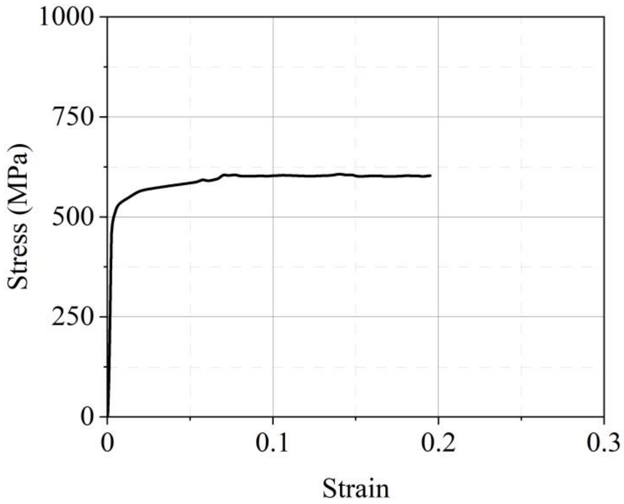

(b)

Figure 3. (a) Steel clamp and (b) tensile stress-strain response of a typical steel clamp.

2.3. Strengthening procedure adopted

Concrete specimens were cast in steel molds with internal dimensions of 150 mm in diameter and 300 mm in height in accordance with (ASTM C943 et al. 2017). The fresh concrete was placed in three equal layers, and each layer was compacted using a vibration table to eliminate entrapped air and ensure proper consolidation. After casting, the specimens were covered with plastic sheets to minimize moisture loss and were demolded after 24 hours. Following demolding, all specimens were water-cured in a controlled curing tank at room temperature (23 ± 2°C) for 28 days. After curing, the specimens were air-dried for 24 hours prior to strengthening.

Strengthening work began once the curing period was completed. Steel clamps were then installed at their designated positions and secured by tightening the screws. A torque wrench was used to ensure uniform tightening across all specimens. Consistent with the procedure used in earlier studies (Ejaz et al. 2025; Rodsin et al. 2022), each clamp was tightened to a torque of 5 N·m to provide standardized confinement conditions. Figure 4 shows the strengthening process.

(a)

(b)

Figure 4. (a) Application of steel clamp at designated location and (b) a completely confined specimen.

2.4. Testing procedures

All compression tests were conducted using a servo-controlled Universal Testing Machine (UTM) with a maximum loading capacity of 2000 kN. Prior to testing, the bearing surfaces of the specimens were carefully ground and leveled to ensure uniform stress distribution. Steel loading plates with a thickness of 25 mm were placed at both ends of each specimen to minimize stress concentration and eccentric loading effects. Axial deformation was measured using two Linear Variable Differential Transformers (LVDTs) with a resolution of 0.001 mm, mounted diametrically opposite on a rigid external frame, as illustrated in Figure 5. The average displacement from both LVDTs was used to calculate axial strain, thereby minimizing the influence of specimen misalignment. Load data were recorded through the UTM's built-in load cell, while displacement data were acquired using a digital data acquisition system synchronized with the testing machine. All signals were continuously monitored and recorded throughout the test. Testing was continued until a significant post-peak strength reduction was observed or until excessive specimen deformation prevented further loading. The axial strain for each loading increment was calculated from the measured displacement divided by the original specimen height.

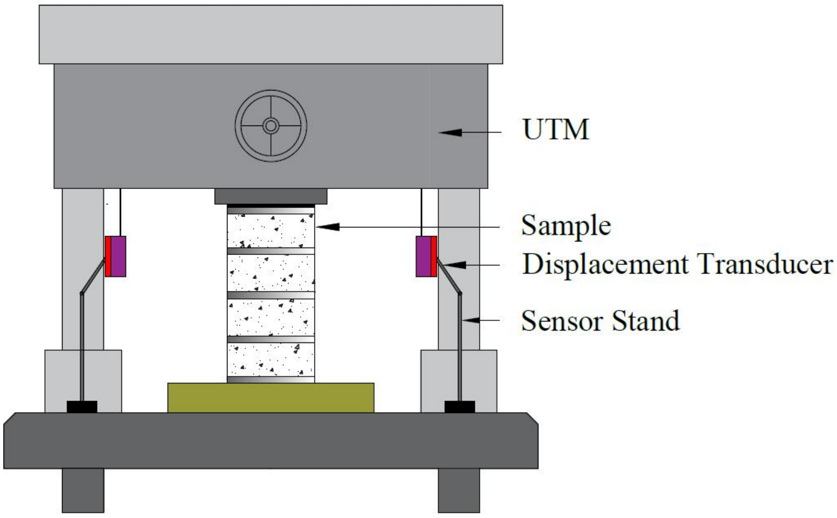

(a)

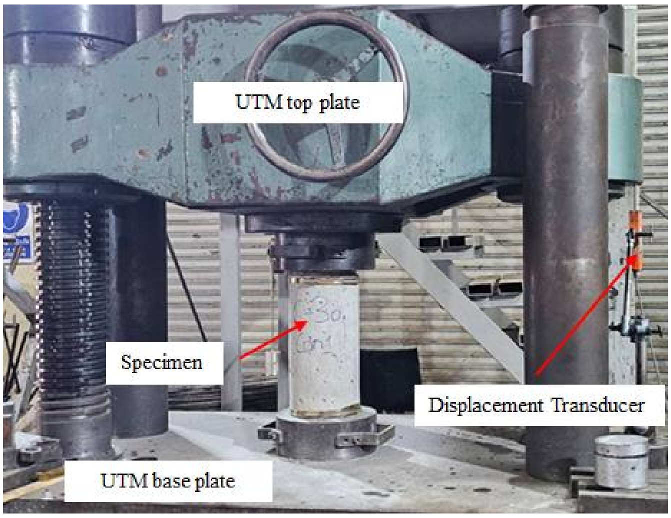

(b)

Figure 5. Test setup illustration: (a) schematics and (b) actual setup.

3. Results

3.1. Failure modes

Figure 6 presents the failure mechanisms observed in all test specimens. For clearer comparison, the failure modes within each group are shown according to their respective confinement levels. In the control specimens, failure was mainly characterized by splitting and crushing. Crushing was most pronounced near the load point, whereas splitting cracks generated along the length of the specimen. Confined specimens showed a regular failure pattern under compressive loads. No visible surface cracks developed before the specimens reached their peak load. After the peak was exceeded, localized bulging appeared in regions of the concrete that were not directly confined by the clamps. This bulging was ascribed to the axial compressive stresses being transferred through the clamps. Throughout loading, the core concrete remained essentially confined until the clamps fractured. These failure characteristics are consistent with observations reported for steel clamp- and batten-confined concrete in previous studies. (Rodsin et al. 2022) reported clamp rupture near fastening zones in circular recycled aggregate concrete columns, while (Ejaz et al. 2025) observed similar localized fracture and progressive confinement loss in square specimens. (Rong and Shi 2020) also documented stress concentration-induced failure in angle-steel confined columns. Compared with these studies on plain concrete, the present RC specimens exhibited more pronounced longitudinal bar buckling and interaction between internal reinforcement and external clamps. The presence of longitudinal steel bars increased post-peak deformation capacity but also intensified local stress demands on the clamps, leading to earlier fracture in some upper regions.

In specimens confined with three steel clamps, lateral protrusion of the concrete was limited. Clamp failure typically occurred at or near the screw connections, and concrete crushing was primarily concentrated in the upper half of the specimen. When five clamps were used, the bulging became more noticeable and more uniformly distributed, reflecting improved confinement compared with the three-clamp configuration. Specimens reinforced with eleven clamps exhibited the most effective confinement, as indicated by extensive crushing and splitting patterns. This behavior indicates that the eleven-clamp setup provided the highest resistance against both concrete crushing and outward deformation. It was also observed that many of the upper clamps failed due to stress concentration in that region. It is noted that the buckling of longitudinal bars was detected in all specimens, regardless of the presence and magnitude of confinement. However, the extent of buckling became more pronounced as the magnitude of confinement increased. This can be attributed to the enhanced buckling demand arising from the improved confinement. Overall, the observed failure mechanisms confirm that steel clamp confinement provides effective restraint up to fracture and that its performance is governed by clamp spacing, fastening details, and interaction with internal reinforcement. These findings further demonstrate the reliability of steel clamps as a passive confinement system while highlighting the importance of proper installation and fastening design for practical applications.

Figure 6. Failure of samples observed in this study.

3.2. Experimental curves

Figure 7 depicts the stress-strain responses for all tested samples, grouped according to their unconfined concrete strengths for improved clarity. The stress-strain curves could be approximated in 2 main segments: (1) an ascending branch that rises to the maximum stress (compressive strength), and (2) a straight descending branch that represents the post-peak degradation. It is important to note that plain concrete specimens under steel clamp confinement had similar features embedded in their stress-strain curves (Ejaz et al. 2025; Rodsin et al. 2022). Across all confinement groups, an evident enhancement in compressive strength was noted. However, the stiffness of the post-peak part, designated as Z, was more gradual compared with that of the corresponding unconfined specimens. The elastic modulus, representing the pre-peak stiffness (up to 40% of compressive strength), remained essentially the same for both confined and related control specimens in all groups. This indicates that the steel clamps acted as passive confinement, becoming effective only after the concrete began to exhibit significant lateral expansion. Because lateral dilation is closely tied to the level of axial compressive strain in the concrete core (Faustino et al. 2016; Hamid et al. 2021), the clamps provided little influence at low strain levels. In addition, the strain at peak strength differed among the various groups, showing that confinement affected both strength and deformation behavior. A detailed quantitative assessment of these parameters is presented in the following sections. An idealized response is also presented in Figure 8. To capture the complete compressive behavior of confined concrete, several key parameters must be approximated. These include the peak strength f_{cc}, the corresponding peak strain ϵ_{cc}, the elastic modulus E_c, and the stiffness of the post-peak degradation part Z. In this study, separate predictive equations for these parameters are developed and presented in Section 4.

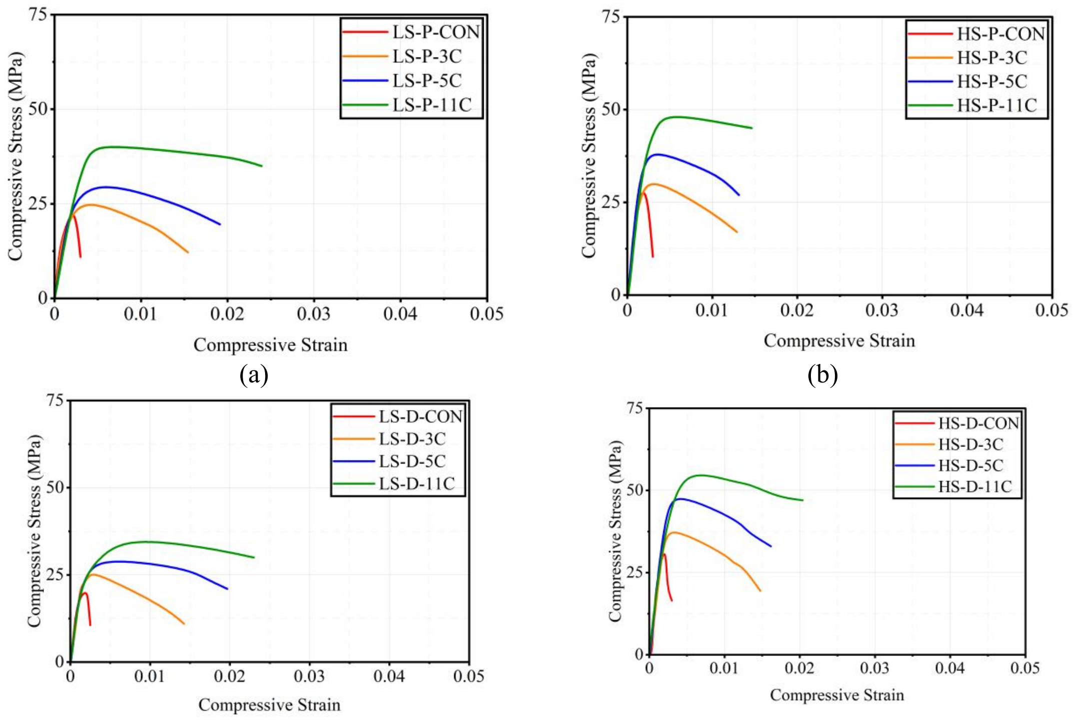

Figure 7. Stress-strain behavior: (a) Subgroup 1A, (b) Subgroup 1B, (c) Subgroup 2A, and (d) Subgroup 2B.

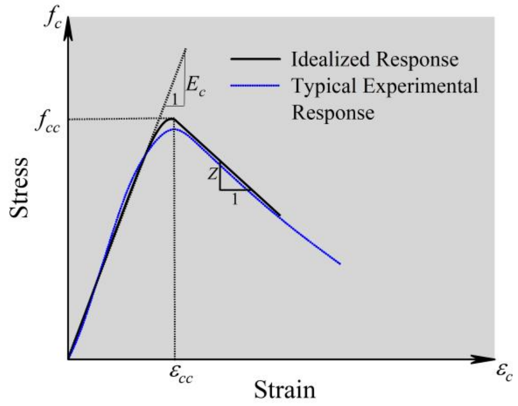

Figure 8. Typical response observed, some key points identified, and an idealized response.

3.3. Compressive strength and related strain comparison

Table 3 presents the average compressive strength and corresponding strain for each sample group, reflecting the mean response of all samples within each category. Overall, all confined groups showed substantial improvements; however, the magnitude of enhancement varied. Subgroup 2A demonstrated the most notable gains, with compressive strength and peak strain increasing by up to 77% and 268%, respectively. It is important to note that the confinement ratio varied in each group. The confinement ratio is defined as the ratio of applied confinement pressure f_l by steel clamps to unconfined compressive strength f_{co} (Thansirichaisree et al. 2024). Studies have shown that the effect of f_{co} on effectiveness of external confinement is detrimental (Saingam et al. 2024b; Tang et al. 2020; Yooprasertchai et al. 2023b). This is because the axial deformation of concrete is compromised by enhancing the compressive strength. As discussed, since the passive confinement is activated under significant lateral dilation which is further related to axial deformation, the reduction in effectiveness of steel clamps is evident.

Table 3. Compressive strength and related strain enhancement.

ID	f_{co} (MPa)	f_{cc} (MPa)	Standard deviation	$\frac{f_{cc}}{f_{co}}$	ϵ_{co}	ϵ_{cc}	Standard deviation	$\frac{\epsilon_{cc}}{\epsilon_{co}}$
LS-P-3C	23.11	27.00	3.12	1.17	0.0020	0.0034	3.124	1.70
LS-P-5C	23.11	31.69	2.26	1.37	0.0020	0.0044	6.254	2.20
LS-P-11C	23.11	40.52	5.67	1.75	0.0020	0.0067	6.987	3.35
HS-P-3C	28.52	32.00	4.25	1.12	0.0022	0.0027	4.698	1.23
HS-P-5C	28.52	39.00	2.12	1.37	0.0022	0.0035	2.365	1.59
HS-P-11C	28.52	49.00	3.14	1.72	0.0022	0.0049	1.987	2.23
LS-D-3C	20.14	25.70	6.50	1.28	0.0019	0.0032	2.365	1.68
LS-D-5C	20.14	29.90	1.35	1.48	0.0019	0.0044	4.698	2.32
LS-D-11C	20.14	35.70	2.65	1.77	0.0019	0.0070	8.741	3.68
HS-D-3C	35.76	39.00	1.36	1.09	0.0023	0.0030	2.236	1.30
HS-D-5C	35.76	49.00	2.65	1.37	0.0023	0.0039	5.145	1.70
HS-D-11C	35.76	56.00	1.55	1.57	0.0023	0.0060	6.254	2.61

A direct comparison between control and confined specimens demonstrates the substantial benefits of steel clamp confinement. For plain-bar specimens, the average compressive strength increased from 23.11 MPa in LS-P-CON to 40.52 MPa in LS-P-11C, representing a 75% improvement, while peak strain increased from 0.0020 to 0.0067 (235% increase). Similarly, for high-strength plain specimens, compressive strength increased from 28.52 MPa to 49.00 MPa (72% increase), accompanied by a 123% increase in peak strain. For specimens reinforced with deformed bars, confinement resulted in even greater enhancements. The compressive strength of LS-D specimens increased from 20.14 MPa to 35.70 MPa (77% increase), while peak strain increased from 0.0019 to 0.0070 (268% increase). In HS-D specimens, compressive strength improved from 35.76 MPa to 56.00 MPa (57% increase), with a corresponding 161% increase in peak strain. These results clearly indicate that steel clamp confinement significantly enhances both strength and deformation capacity compared with unconfined specimens.
For calculating the confinement pressure, the widely adopted approach presented by (Mander et al.1988) was modified to suit the steel clamp configuration utilized in this work. Each steel clamp had a width of

10 mm and a thickness of 1.2 mm. The center-to-center spacing for the 3-, 5-, and 11-clamp configurations was 66 mm, 44 mm, and 24 mm, respectively, corresponding to clear spacings of 54 mm, 32 mm, and 14 mm. Since the confinement provided by discrete clamps is not continuous, the effective confinement pressure between consecutive clamp levels must be reduced to account for the non-uniform distribution of lateral restraint. For this purpose, an effectiveness coefficient k_e was introduced, like the method of (Mander et al. 1988), as shown in Figure 9. The effective lateral confinement stress acting on the concrete was then determined using equation (1), expressed as:

$$f_l' = \frac{1}{2} k_e \rho_s f_{yh} \tag{1}$$

where k_e, ρ_s, and f_{yh} represent the confinement efficiency, the ratio of the volumes of steel clamps (per center-to-center spacing) to that of concrete, and the yield capacity of the steel clamps, respectively. These parameters may be given in equations (2) and (3).

$$k_e = \frac{A_e}{A_c} = \frac{\frac{\pi}{4} d_s^2 \left[1 - \frac{s'}{2d_s}\right]^2}{\frac{\pi d_s^2}{4}} \tag{2}$$

$$\rho_s = \frac{A_{sc} \pi d_s}{\frac{\pi}{4} d_s^2 s} = \frac{4A_{sc}}{d_s s} \tag{3}$$

where A_e is the effective area of confined concrete at the midpoint among steel clamp levels, d_s is the cylinder diameter, A_{sc} is the cross-sectional area of a single clamp, s is the center-to-center spacing of the clamps, and A_c cross-sectional area of concrete. The effective confining pressures for the 3-, 5-, and 11-clamp configurations were determined as 1.53 MPa, 2.72 MPa, and 5.64 MPa, respectively.

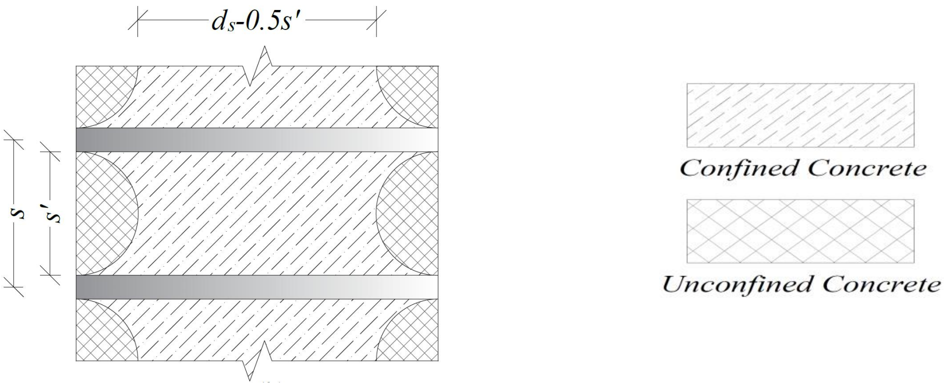

Figure 9. Assumed variation in confinement along the height of sample.

As shown in Figure 10, the confinement ratio effect is shown on both normalized compressive strength and related strain (confined samples). It is interesting to observe that both compressive strength and related strain are enhanced by improving the confinement ratio. From this visual observation, the trend seems to follow a parabolic curve in both cases. Interestingly, specimens with plain and deformed bars seem to follow the same trend and it could be deduced that the kind of internal reinforcement does not impact the axial capacity of confined specimens. Moreover, the corresponding ductility is also not affected by the kind of internal reinforcement. Based on these findings, the corresponding modeling is adopted. It is seen that specimens with deformed bars offered the wider range of confinement ratios (shown by circular points in Figure 10). Therefore, deformed bar specimens were used for statistical modeling, whereas the proposed models in Section 4 will be verified for both Group 1 and Group 2 specimens.

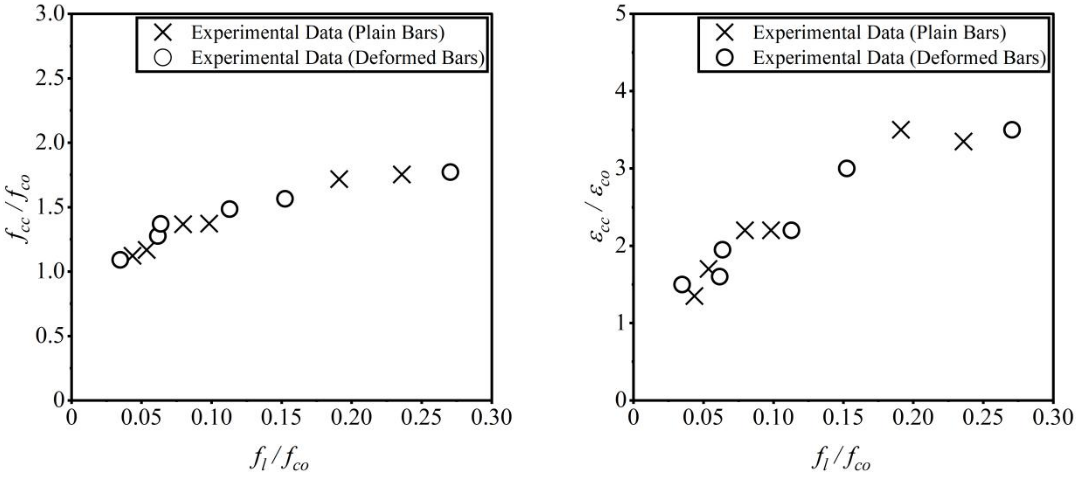

(a) (b)

Figure 10. Effect of confinement ratio on normalized: (a) compressive strength and (b) related strain.

3.4. Dissipated energy and ultimate strain

The ultimate strain is given as the strain that corresponds to a 50% decrease from the peak compressive strength (Yang et al. 2014). The dissipated energy was calculated as the area under stress-strain curves up to this ultimate strain. Table 4 provides the calculated values of these parameters. In Group 1, up to 722.22% and 440.74% enhancement in ultimate strain was noted for LS and HS type specimens, respectively. Likewise, the enhancement in ultimate strain was observed for all magnitudes of steel clamp confinement. Similarly, up to 900% and 786.86% enhancement in ultimate strain was noted for Group 2 LS and HS specimens, respectively. Interestingly, the improvement in dissipated energy was more pronounced with Group 1 LS and HS specimens showing up to 902.08% and 1173.47%, respectively. While Group 2 LS and HS specimens demonstrated this improvement by up to 2017.65% and 1978.72%, respectively.

Table 4. Compressive strength and related strain enhancement.

ID	Ultimate Strain	Enhancement in Ultimate Strain	Dissipated Energy (MPa)	Enhancement in Dissipated Energy
LS-P-CON	0.0027	-	0.048	-
LS-P-3C	0.0101	274.07	0.221	360.42
LS-P-5C	0.0131	385.19	0.343	614.58
LS-P-11C	0.0222	722.22	0.481	902.08
HS-P-CON	0.0026	-	0.049	-
HS-P-3C	0.0082	203.70	0.214	336.73
HS-P-5C	0.0112	314.81	0.281	473.47
HS-P-11C	0.0146	440.74	0.624	1173.47
LS-D-CON	0.0023	-	0.034	-
LS-D-3C	0.0071	208.70	0.151	344.12
LS-D-5C	0.0169	634.78	0.446	1211.76
LS-D-11C	0.0230	900.00	0.720	2017.65
HS-D-CON	0.0023	-	0.047	-
HS-D-3C	0.0106	360.87	0.335	612.77
HS-D-5C	0.0125	443.48	0.512	989.36
HS-D-11C	0.0204	786.96	0.977	1978.72

Compared with control specimens, steel clamp confinement led to remarkable improvements in ductility and energy absorption capacity. In Group 1 (plain bars), ultimate strain increased from 0.0027 in LS-P-CON to 0.0222 in LS-P-11C, corresponding to a more than sevenfold increase, while dissipated energy increased from 0.048 MPa to 0.481 MPa (over 900% improvement). For HS-P specimens, dissipated energy increased from 0.049 MPa to 0.624 MPa, representing an enhancement of approximately 1170%. In Group 2 (deformed bars), ultimate strain increased from 0.0023 in LS-D-CON to 0.0230 in LS-D-11C (900% increase), while dissipated energy increased from 0.034 MPa to 0.720

MPa (over 2000% increase). Similar trends were observed in HS-D specimens, confirming that steel clamp confinement significantly improves post-peak deformation capacity and energy dissipation compared with unconfined concrete.

4. Analytical modeling

This part presents the derivation of expressions for estimating the compressive strength, strain at peak strength, and post-peak stiffness Z of concrete confined with steel clamps. Earlier results showed that improvements in both peak strength and the corresponding strain are governed by the concrete's confinement ratio. These factors were therefore employed to establish the full compressive stress-strain relationship for concrete confined by steel clamp. Since the proposed confinement method is novel in sense that it has not previously been applied to RC sections, conventional passive confinement models cannot accurately capture the distinct behavior of steel clamps. In this regard, the modeling approach proposed by (Popovics et al. 1973) was found to best represent the ascending portion of the compressive response. Notably, Eq. (4) has also been utilized by (Cusson and Paultre et al.1995) to characterize the stress-strain behavior of internally confined concrete.

$$f_c = f_{cc}\left[\frac{k\left(\frac{\epsilon_c}{\epsilon_{cc}}\right)}{k-1+\left(\frac{\epsilon_c}{\epsilon_{cc}}\right)^k}\right] \quad for\ \epsilon_c \le \epsilon_{cc} \tag{4}$$

$$k = \frac{E_c}{E_c - \frac{f_{cc}}{\epsilon_{cc}}} \tag{5}$$

In Equations (4) and (5), the elastic stiffness of concrete E_c is determined determined by expression suggested by ACI 318 (ACI Committee 318 et al. 2019) for normal strength concrete, i.e., $E_c = 4700\sqrt{f_{co}}$ in MPa.

4.1. Proposed expression for confined compressive strength f_{cc}

Section 3 showed that the confinement ratio f_l/f_{co} had a positive impact on the enhancement of the peak compressive strength f_{cc} of steel clamp-confined concrete. The increase in f_{cc} was found to be unaffected by the type of internal reinforcement used in the specimens. It was further noted that the specimens reinforced with deformed bars exhibited the largest range of confinement ratios. Since both deformed-bar and plain-bar specimens demonstrated a similar trend with respect to the confinement ratio, only the deformed-bar specimens were used in formulating the proposed expressions, while the resulting equations were later validated for both reinforcement types. Using nonlinear regression utilizing the Gauss–Newton method, Eq. (6) is proposed.

$$\frac{f_{cc}}{f_{co}} = 1 + 1.942\left(\frac{f_l}{f_{co}}\right)^{0.676} \tag{6}$$

The proposed Eq. (6) achieved a coefficient of determination $R^2 = 0.93$, showing a strong correlation between the predicted and experimental findings. As illustrated in Figure 11(a), the equation effectively captures the experimentally observed enhancement in compressive strength, demonstrating its suitability for modeling the response of steel clamp-confined concrete.

4.2. Proposed expression for strain at confined compressive strength ϵ_{cc}

Similarly, the confinement ratio exerted a significant influence on the strain at peak strength. The strain at peak strength, ε_{cc}, is a key parameter in defining the compressive stress-strain response of concrete, as illustrated in Figure 8. Considering the relevant independent variables, Eq. (7) is proposed as follows:

$$\frac{\epsilon_{cc}}{\epsilon_{co}} = 1 + 7.201\left(\frac{f_l}{f_{co}}\right)^{0.777} \tag{7}$$

The proposed Eq. (8) yielded an R^2 value of 0.94, and its efficiency is illustrated in Figure 11(b). This equation closely captures the experimentally observed improvement in the strains at peak strength.

4.3. Proposed expression post-peak modulus Z

From Section 3, it was observed that the degree of post-peak strength reduction declined as the level of steel clamp confinement improved, as illustrated in Figure 7. Furthermore, higher unconfined concrete strength also contributed to a slower rate of strength degradation. To quantify this behavior, Eq. (9) is presented to predict the post-peak degradation slope Z as:

$$Z = -159.017 \times \left[f_{co} + \frac{f_{co}}{\left(\frac{f_l}{f_{co}}\right)^{80.510}} \right]^{0.009} \tag{9}$$

The proposed Eq. (9) also yielded an R^2 value of 0.94, and its effectiveness is illustrated in Figure 11(c). This equation closely captures the experimentally observed strength degradation after achieving the compressive strength. Importantly, it is observed from Figure 11 that although proposed expressions were regression-derived from data of specimens with deformed bars only, these expressions could also trace the trend of improvement in compressive strength, corresponding strain, and post-peak moduli of specimens with plain bars as well.

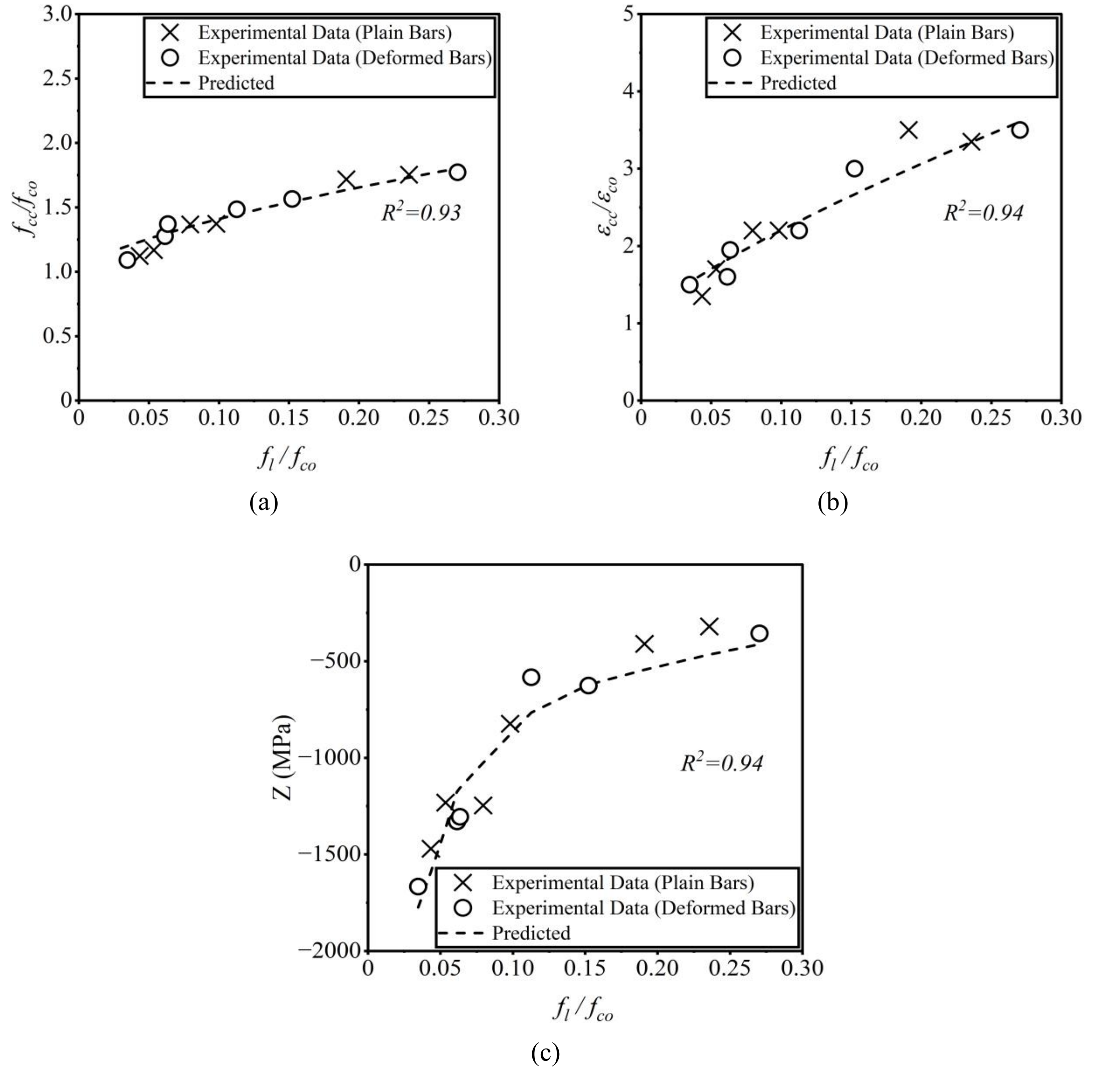

Figure 11. Comparison of experimental parameters with predicted trend as a function of confinement ratio: (a) compressive strength, (b) strain at compressive strength, and (c) post-peak elastic modulus.

4.4. Comparison of experimental response with predicted curves

Figure 12 presents a systematic comparison between the experimentally measured and analytically predicted compressive stress–strain responses for all specimen groups. The comparison indicates that the proposed model accurately reproduces the key stages of behavior, including the initial elastic response, peak compressive strength, corresponding peak strain, and post-peak degradation. For all confinement levels, the predicted peak strength and peak strain closely matched the experimental values, with only minor deviations observed in the post-peak region.

It is repeated that the proposed approach was based on experimental data of specimens in Group 2 only, i.e., specimens with deformed bars only. However, since plain and deformed bar specimens were found to follow a similar trend vs confinement ratio, the proposed method was supposed to predict the response of specimens in Group 1 as well. It is important to note that the predicted response in the post-peak region was terminated when a 20% reduction in compressive strength was achieved. Figure 12(a) and 12(b) confirm that the proposed method and expressions, though derived from deformed bar specimens, are able to predict the response of specimens with plain bars as well. The expressions proposed in this study follow the same practical formulation style adopted in ACI 440 (ACI Committee 440 rt al. 2017), ensuring familiarity and ease of use for practicing engineers. As a result, engineers experienced with ACI 440 procedures can readily apply the developed model without requiring additional modifications or specialized interpretation. Compared with existing confinement models developed for FRP-confined concrete e.g., (Lim and Ozbakkaloglu et al.2014; Ozbakkaloglu et al. 2013) and steel-based confinement systems (Rodsin et al. 2022; Rong and Shi 2020), the present model offers improved consistency in capturing post-peak behavior for discrete steel clamp configurations. While many conventional models primarily focus on peak strength enhancement, they often underestimate post-peak ductility for discontinuous confinement systems. In contrast, the proposed approach explicitly incorporates the influence of confinement ratio on post-peak stiffness, enabling more accurate representation of strength degradation. Despite the good predictive performance, the proposed model has certain limitations. The regression-based expressions were derived from a limited experimental dataset involving cylindrical specimens under monotonic axial loading. The effects of cyclic loading, eccentric compression, long-term degradation, and large-scale structural behavior were not considered. Therefore, the proposed model should be applied with caution beyond the investigated parameter ranges. Further experimental and numerical studies are recommended to extend its applicability.

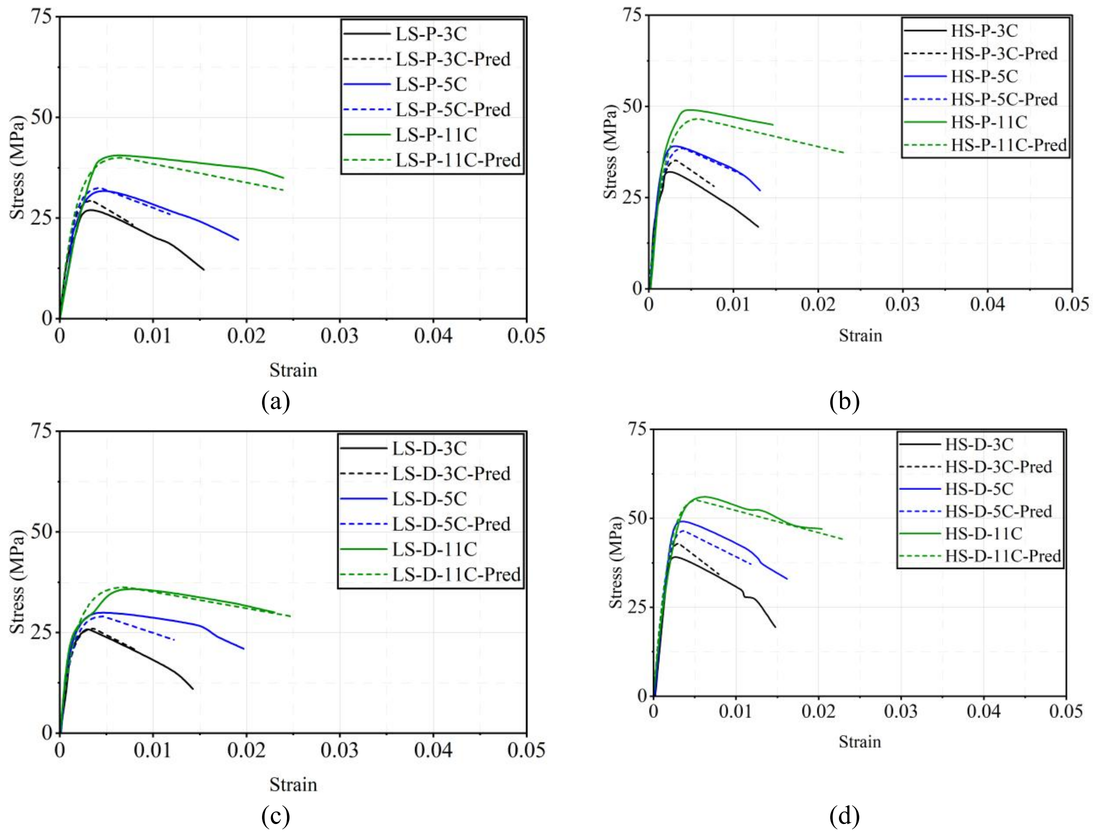

Figure 12. Comparison of predicted and experimental response: (a) Subgroup 1A, Subgroup 1B, Subgroup 2A, and (d) Subgroup 2B.

4.5. Model validation and uncertainty analysis

To evaluate the predictive performance of the proposed regression-based models, statistical validation was conducted using standard error indices, including the mean absolute percentage error (MAPE), root mean square error (RMSE), and mean bias error (MBE).

Table 5 provides the calculated values of these parameters. For peak compressive strength prediction, the model achieved a MAPE of 4.21% and an RMSE of 0.065, indicating excellent agreement between experimental and predicted values. The prediction of strain at peak strength also showed good accuracy, with a MAPE of 7.34% and an RMSE of 0.219. These results confirm the reliability of the proposed expressions in capturing both strength and deformation characteristics.

For the post-peak stiffness parameter Z, a relatively higher MAPE of 17.13% was obtained, reflecting the inherent variability associated with post-peak behavior and damage localization. Nevertheless, the model was able to capture the overall degradation trend with acceptable accuracy.

The mean bias errors for all parameters remained close to zero, indicating the absence of significant systematic overestimation or underestimation. Overall, the validation results demonstrate that the proposed analytical expressions provide reliable and robust predictions within the investigated parameter range.

Table 5. Statistical validation of proposed regression models.

Parameter	R^2	MAPE (%)	RMSE	MBE
f_{cc}/f_{co}	0.93	4.21	0.065	0.012
$\epsilon_{cc}/\epsilon_{co}$	0.94	7.33	0.218	-0.030
Z	0.94	17.13	140.101	-56.560

5. Conclusions

In this study, RC specimens with varying unconfined strengths and different numbers of steel clamps were cast and tested under axial compression. Both plain and deformed longitudinal reinforcement were included. The mechanical properties of the steel clamps were characterized through tensile testing. All concrete specimens were cast, cured, confined with steel clamps, and instrumented with LVDTs to measure axial deformation. The compressive response, including peak strength, strain at peak, post-peak behavior, and failure modes, was recorded and analyzed for each specimen. The following conclusions were derived.

1. Steel clamp confinement significantly enhanced the compressive performance of reinforced concrete by improving strength, ductility, and energy dissipation. Peak compressive strength, strain at peak strength, ultimate strain, and dissipated energy increased by up to 77%, 268%, 900%, and nearly 2000%, respectively, compared with unconfined specimens
2. The stress-strain analysis revealed that steel clamp confinement notably improved the compressive strength of concrete while leaving the initial elastic modulus largely unchanged, confirming its role as a passive confinement system.
3. The results indicate that steel clamp confinement extensively improved both compressive strength and peak strain across all specimen groups, with subgroup 2A showing the largest gains of 77% and 268%, respectively. The effectiveness of confinement was influenced by the confinement ratio (f_l/f_{co}), with higher unconfined concrete strength reducing the relative enhancement. This reduction occurs because passive steel clamp confinement is activated only under substantial lateral dilation, which is constrained in higher-strength concrete, highlighting the interaction between concrete strength and confinement effectiveness.
4. Regression-based predictive expressions were developed to estimate peak strength, peak strain, and post-peak stiffness, enabling accurate simulation of the full stress–strain response of steel clamp-confined concrete. The proposed model demonstrated strong agreement with experimental results and was applicable to both plain- and deformed-bar specimens

This study was limited to small-scale specimens, specifically cylindrical samples with a diameter of 150 mm and a length of 300 mm, aimed at developing material models under monotonic axial load. The findings may not fully translate to larger-scale applications or real-world scenarios. Further studies should focus on large-scale columns subjected to lateral cyclic loads to better understand the performance and effectiveness of steel clamp confinement in more complex loading conditions. This would enhance the applicability and reliability of the proposed material models. Although the present study demonstrates the effectiveness of steel clamp confinement for enhancing the compressive performance of RC, several aspects warrant further investigation. Future research should examine the long-term durability of steel clamps under environmental exposure, including corrosion, temperature variation, and moisture effects. The behavior of steel clamp-confined RC members under cyclic and seismic loading conditions should also be explored to assess their applicability in earthquake-resistant design. In addition, the influence of different clamp materials, geometries, and fastening systems on confinement efficiency deserves systematic evaluation. Further studies involving full-scale structural members, such as columns and bridge piers, are recommended to validate the proposed model under realistic boundary conditions and loading scenarios. Moreover, numerical modeling and parametric analyses could be conducted to optimize clamp spacing and installation procedures. These efforts would contribute to refining the design guidelines and expanding the practical application of steel clamp confinement in structural rehabilitation and strengthening projects. Additional sources of uncertainty include potential misalignment during loading, variations in concrete mixing and curing processes, and differences in the mechanical properties of the steel clamps, all of which could impact the experimental results and their generalizability.

Author Contributions

Conceptualization, K.R., A.E., G.S., T.M. and Q.H.; methodology, K.R., C.B., A.E., P.C., C.S.; software, C.B., B.C., G.S., P.C. ,C.S.; validation, K.R., Q.H, C.S. and T.M.; formal analysis, K.R., A.E, G.S., Q.H, C.S.; investigation, K.R., C.S., B.C., T.M.; resources, C.B., P.C., C.S.; data curation, P.C., B.C., G.S.; writing—original draft preparation, K.R., C.B., P.C.; writing—review and editing, A.E., B.C., G.S., T.M., Q.H., P.C., C.S.; visualization, A.E., T.M., Q.H.; supervision, P.C., C.S., Q.H.; project administration, C.B., P.C., C.S.; funding acquisition, C.B. All authors have read and agreed to the published version of the manuscript.

Funding

This research was funded by College of Industrial Technology, King Mongkut's University of Technology, North Bangkok (Grant No. Res-CIT-IL032/2025).

Conflict of Interest Statement

The authors declare no conflicts of interest.

Data Availability Statement

The data supporting the findings of this study are available from the corresponding author upon reasonable request.

Acknowledgement

This research was funded by College of Industrial Technology, King Mongkut's University of Technology, North Bangkok (Grant No. Res-CIT-IL032/2025). Thanks are also extended to AIT, Thailand for supporting test facilities.

References

Aboutaha, R. S., M. U. Engelhardt, J. O. Jirsa, and M. F. Kreger. 1996. "Retrofit of Concrete Columns with Inadequate Lap splices by the Use of Rectangular Steel Jackets." *Earthquake Spectra*, 12 (4): 693–714. Earthquake Engineering Research Institute. https://doi.org/10.1193/1.1585906.

ACI Committee 318. 2019. *ACI 318-19: Building Code Requirements for Structural Concrete and Commentary*. Farmington Hills, MI, USA.

ACI Committee 440. 2017. "Guide for the Design and Construction of Externally bonded FRP systems for strengthening concrete structures."

Aljohani, A., A. Aloufi, A. A. Qazali, H. Babkair, O. Qadiri, and H. T. Fadel. 2025. "Allergic Contact Dermatitis From Dental Bonding Materials Containing Methacrylate: A Report of Two Cases." *Cureus*, 17 (5): e84395. Springer Science and Business Media LLC. https://doi.org/10.7759/CUREUS.84395.

Askar, M. K., A. F. Hassan, and Y. S. S. Al-Kamaki. 2022. "Flexural and shear strengthening of reinforced concrete beams using FRP composites: A state of the art." *Case Studies in Construction Materials*, e01189. Elsevier. https://doi.org/10.1016/J.CSCM.2022.E01189.

ASTM C943. 2017. "Standard practice for making test cylinders and prisms for determining strength and density of preplaced-aggregate concrete in the laboratory."

ASTM E8/E8M-21. 2021. "Standard Test Methods for Tension Testing of Metallic Materials."

Attari, N., S. Amziane, and M. Chemrouk. 2012. "Flexural strengthening of concrete beams using CFRP, GFRP and hybrid FRP sheets." *Construction and Building Materials*, 37: 746–757. Elsevier. https://doi.org/10.1016/J.CONBUILDMAT.2012.07.052.

Baggio, D., K. Soudki, and M. Noël. 2014. "Strengthening of shear critical RC beams with various FRP systems." *Construction and Building Materials*, 66: 634–644. Elsevier. https://doi.org/10.1016/J.CONBUILDMAT.2014.05.097.

Bournas, D. A., and T. C. Triantafillou. 2011. "Bond Strength of Lap-Spliced Bars in Concrete Confined with Composite Jackets." *Journal of Composites for Construction*, 15 (2): 156–167. American Society of Civil Engineers. https://doi.org/10.1061/(ASCE)CC.1943-5614.0000078.

Bousias, S., A. Spathis, and M. Fardis. 2004. "Seismic retrofitting of columns with lap-splices through CFRP jackets." In: *13th World Conference on Earthquake Engineering*. Vancouver, B.C., Canada.

Chai, Y. H., M. J. N. Priestley, and F. Seible. 1991. "Seismic Retrofit of Bridge Columns by Steel Jacketing." In: *Bridge Engineering Conference, Transportation Research Record No. 1290*. Denver, Colorado.

Chang, S. Y., T. W. Chen, N. C. Tran, and W. I. Liao. 2014. "Seismic Retrofitting of RC Columns with RC Jackets and Wing Walls with Different Structural Details." *Earthquake Engineering and Engineering Vibration*, 13 (2): 279–292. Institute of Engineering Mechanics (IEM). https://doi.org/10.1007/S11803-014-0230-4.

Chen, J. F., and J. G. Teng. 2003. "Shear capacity of FRP-strengthened RC beams: FRP debonding." *Construction and Building Materials*, 17 (1): 27–41. Elsevier. https://doi.org/10.1016/S0950-0618(02)00091-0.

Cusson, D., and P. Paultre. 1995. "Stress-Strain Model for Confined High-Strength Concrete." *Journal of Structural Engineering*, 121 (3): 468–477. American Society of Civil Engineers. https://doi.org/10.1061/(ASCE)0733-9445(1995)121:3(468).

Daudey, X., and A. Filiatrault. 2011. "Seismic Evaluation and Retrofit with Steel Jackets of Reinforced Concrete Bridge Piers Detailed with Lap-Splices." *Canadian Journal of Civil Engineering*, 27 (1): 1–16. NRC Research Press Ottawa, Canada . https://doi.org/10.1139/L99-029.

Dong, J., Q. Wang, D. He, and Z. Guan. 2011. "CFRP sheets for flexural strengthening of RC beams." *2011 International Conference on Multimedia Technology, ICMT 2011*, 1000–1003. https://doi.org/10.1109/ICMT.2011.6003160.

Ejaz, A., A. Ruangrassamee, T. Jirawattanasomkul, and D. Zhang. 2025. "Experimental and analytical investigations on enhancing compressive stress vs. strain response of square-section recycled brick aggregate concrete by steel clamps." *Case Studies in Construction Materials*, 22: e04645. Elsevier. https://doi.org/10.1016/J.CSCM.2025.E04645.

Ejaz, A., A. Ruangrassamee, P. Kruavit, P. Udomworarat, and A. C. Wijeyewickrema. 2022. "Strengthening of Substandard Lap Splices Using Hollow Steel Section (HSS) Collars." *Structures*, 46: 128–145. Elsevier. https://doi.org/10.1016/J.ISTRUC.2022.10.030.

ElGawady, M., M. Endeshaw, D. McLean, and R. Sack. 2009. "Retrofitting of Rectangular Columns with Deficient Lap Splices." *Journal of Composites for Construction*, 14 (1): 22–35. American Society of Civil Engineers. https://doi.org/10.1061/(ASCE)CC.1943-5614.0000047.

Erfan, A. M., R. M. A. Elnaby, A. A. Badr, and T. A. El-sayed. 2021. "Flexural behavior of HSC one way slabs reinforced with basalt FRP bars." *Case Studies in Construction Materials*, 14: e00513. Elsevier. https://doi.org/10.1016/J.CSCM.2021.E00513.

Farghaly, A. S., and B. Benmokrane. 2013. "Shear behavior of FRP-reinforced concrete deep beams without web reinforcement." *Journal of Composites for Construction*, 17 (6): 04013015. American Society of Civil Engineers (ASCE). https://doi.org/10.1061/(ASCE)CC.1943-5614.0000385.

Faruk, O., A. K. Bledzki, H. P. Fink, and M. Sain. 2012. "Biocomposites reinforced with natural fibers: 2000–2010." *Progress in Polymer Science*, 37 (11): 1552–1596. Pergamon. https://doi.org/10.1016/J.PROGPOLYMSCI.2012.04.003.

Faustino, P., P. Frade, and C. Chastre. 2016. "Lateral Cyclic Behaviour of RC Columns Confined With Carbon Fibres." *Structures*, 5: 196–206. Elsevier. https://doi.org/10.1016/J.ISTRUC.2015.11.004.

Gao, C., L. Huang, L. Yan, R. Jin, and B. Kasal. 2019. "Strength and ductility improvement of recycled aggregate concrete by polyester FRP-PVC tube confinement." *Composites Part B: Engineering*, 162: 178–197. Elsevier. https://doi.org/10.1016/J.COMPOSITESB.2018.10.102.

Gao, Z. Y., S. S. Zhang, G. Lin, T. Yu, and X. F. Nie. 2024. "Compressive behavior of FRP-confined normal concrete or seawater sea-sand concrete containing FRP-bar recycled coarse aggregates." *Engineering Structures*, 303: 117500. Elsevier. https://doi.org/10.1016/J.ENGSTRUCT.2024.117500.

Ghosh, K. K., and S. A. Sheikh. 2007. "Seismic Upgrade with Carbon Fiber-Reinforced Polymer of Columns Containing Lap-Spliced Reinforcing Bars." *ACI Structural Journal*, 104 (2): 227–236. https://doi.org/10.14359/18535.

Gu, D. S., Y. F. Wu, G. Wu, and Z. S. Wu. 2012. "Plastic hinge analysis of FRP confined circular concrete columns." *Construction and Building Materials*, 1 (27): 223–233. https://doi.org/10.1016/J.CONBUILDMAT.2011.07.056.

Hamid, F. L., G. B. Jumaa, and S. S. Weli. 2021. "Predicting ultimate strength of FRP and lateral steel confined circular concrete columns using Artificial Neural Networks." *Asian Journal of Civil Engineering*, 22 (3): 493–503. Springer Science and Business Media Deutschland GmbH. https://doi.org/10.1007/S42107-020-00328-X/FIGURES/25.

Haroun, M. A., and H. M. Elsanadedy. 2005. "Fiber-Reinforced Plastic Jackets for Ductility Enhancement of Reinforced Concrete Bridge Columns with Poor Lap-Splice Detailing." *Journal of Bridge Engineering*, 10 (6): 749–757. American Society of Civil Engineers. https://doi.org/10.1061/(ASCE)1084-0702(2005)10:6(749).

Harries, K., J. Ricles, S. Pissiki, and R. Sause. 2006. "Seismic Retrofit of Lap Splices in Nonductile Columns Using CFRP Jackets." *ACI Structural Journal*, 103 (6): 226–236. American Concrete Institute. https://doi.org/10.14359/18242.

Jamatia, R., and A. Deb. 2017. "Size Effect in FRP-Confined Concrete under Axial Compression." *Journal of Composites for Construction*, 21 (6): 04017045. American Society of Civil Engineers. https://doi.org/10.1061/(ASCE)CC.1943-5614.0000825.

Jiang, C., F. Yuan, Y.-F. Wu, and X.-M. Zhao. 2019. "Effect of Interfacial Bond on Plastic Hinge Length of FRP-Confined RC Columns." *Journal of Composites for Construction*, 23 (2): 04019007. American Society of Civil Engineers. https://doi.org/10.1061/(ASCE)CC.1943-5614.0000932.

Jiang, T., X. M. Wang, W. P. Zhang, G. M. Chen, and Z. H. Lin. 2020. "Behavior of FRP-Confined Recycled Brick Aggregate Concrete under Monotonic Compression." *Journal of Composites for Construction*, 24 (6): 04020067. American Society of Civil Engineers (ASCE). https://doi.org/10.1061/(ASCE)CC.1943-5614.0001080/ASSET/BEECB465-A7D2-4E8F-AEE6-D3BC22D6CD95/ASSETS/IMAGES/LARGE/CCENG-3036F14.JPG.

Juntanalikit, P., T. Jirawattanasomkul, and A. Pimanmas. 2016. “Experimental and numerical study of strengthening non-ductile RC columns with and without lap splice by Carbon Fiber Reinforced Polymer (CFRP) jacketing.” *Engineering Structures*, 125: 400–418. Elsevier. https://doi.org/10.1016/J.ENGSTRUCT.2016.07.019.

Khalid Ali, O., A. Ismail Al-Hadithi, and A. Tareq Noaman. 2022. “Flexural performance of layered PET fiber reinforced concrete beams.” *Structures*, 35: 55–67. Elsevier. https://doi.org/10.1016/J.ISTRUC.2021.11.007.

Kodur, V. K. R., M. Z. Naser, and H. S. Kim. 2025. “Fire performance of concrete structures incorporating FRP reinforcement: State-of-the-art and knowledge gaps.” *Cement and Concrete Composites*, 161: 106074. Elsevier. https://doi.org/10.1016/J.CEMCONCOMP.2025.106074.

Lehman, D. E., S. E. Gookin, A. M. Nacamull, and J. P. Moehle. 2001. “Repair of Earthquake-Damaged Bridge Columns.” *ACI Structural Journal*, 98 (2): 233–242. https://doi.org/10.14359/10192.

Lim, J. C., and T. Ozbakkaloglu. 2014. “Confinement Model for FRP-Confined High-Strength Concrete.” *Journal of Composites for Construction*, 18 (4): 04013058. American Society of Civil Engineers (ASCE). https://doi.org/10.1061/(ASCE)CC.1943-5614.0000376/ASSET/5EEBC253-2F33-4DE5-A6C8-B11ADF575EFE/ASSETS/IMAGES/LARGE/FIGURE9.JPG.

Mander, J. B., M. J. N. Priestley, and R. Park. 1988. “Theoretical StressStrain Model for Confined Concrete.” *Journal of Structural Engineering*, 114 (8): 1804–1826. American Society of Civil Engineers. https://doi.org/10.1061/(ASCE)0733-9445(1988)114:8(1804).

Munir, M. J., S. M. S. Kazmi, Y. F. Wu, and X. Lin. 2021. “Axial stress-strain performance of steel spiral confined acetic acid immersed and mechanically rubbed recycled aggregate concrete.” *Journal of Building Engineering*, 34: 101891. Elsevier. https://doi.org/10.1016/J.JOBE.2020.101891.

Ozbakkaloglu, T., J. C. Lim, and T. Vincent. 2013. “FRP-confined concrete in circular sections: Review and assessment of stress–strain models.” *Engineering Structures*, 49: 1068–1088. Elsevier. https://doi.org/10.1016/J.ENGSTRUCT.2012.06.010.

Park, T. W., U. J. Na, L. Chung, and M. Q. Feng. 2008. “Compressive behavior of concrete cylinders confined by narrow strips of CFRP with spacing.” *Composites Part B: Engineering*, 39 (7–8): 1093–1103. Elsevier. https://doi.org/10.1016/J.COMPOSITESB.2008.05.002.

Pickering, S. J. 2006. “Recycling technologies for thermoset composite materials—current status.” *Composites Part A: Applied Science and Manufacturing*, 37 (8): 1206–1215. Elsevier. https://doi.org/10.1016/J.COMPOSITESA.2005.05.030.

Popovics, S. 1973. “A Numerical Approach to the Complete Stress-Strain Curve of Concrete.” *Cement and Concrete Research*, 3 (5): 583–599. Pergamon. https://doi.org/10.1016/0008-8846(73)90096-3.

Priestley, M. J. N., and F. Seible. 1995. “Design of Seismic Retrofit Measures for Concrete and Masonry Structures.” *Construction and Building Materials*, 9 (6): 365–377. Elsevier. https://doi.org/10.1016/0950-0618(95)00049-6.

Raza, S., M. K. I. Khan, S. J. Menegon, H. H. Tsang, and J. L. Wilson. 2019. “Strengthening and Repair of Reinforced Concrete Columns by Jacketing: State-of-the-Art Review.” *Sustainability 2019, Vol. 11, Page 3208*, 11 (11): 3208. Multidisciplinary Digital Publishing Institute. https://doi.org/10.3390/SU11113208.

del Rey Castillo, E., M. Griffith, and J. Ingham. 2018. “Seismic behavior of RC columns flexurally strengthened with FRP sheets and FRP anchors.” *Composite Structures*, 203: 382–395. Elsevier. https://doi.org/10.1016/J.COMPSTRUCT.2018.07.029.

Rodsin, K., P. Joyklad, Q. Hussain, H. Mohamad, A. Buatik, M. Zhou, K. Chaiyasarn, A. Nawaz, T. Mehmood, and A. ELNEMR. 2022. “Behavior of steel clamp confined brick aggregate concrete circular columns subjected to axial compression.” *Case Studies in Construction Materials*, 16: e00815. Elsevier. https://doi.org/10.1016/J.CSCM.2021.E00815.

Rong, C., and Q. Shi. 2020. “Behaviour of angle steel frame confined concrete columns under axial compression.” *Construction and Building Materials*, 241: 118034. Elsevier. https://doi.org/10.1016/J.CONBUILDMAT.2020.118034.

Rousakis, T. C., A. I. Karabinis, and P. D. Kiousis. 2007. “FRP-confined concrete members: Axial compression experiments and plasticity modelling.” *Engineering Structures*, 29 (7): 1343–1353. Elsevier. https://doi.org/10.1016/J.ENGSTRUCT.2006.08.006.

Saingam, P., C. K. Gadagamma, Q. Hussain, H. H. Hlaing, R. Suwannatrai, M. I. Qureshi, K. Khan, and A. Ejaz. 2025. “Modeling and comparative analysis of sustainable cotton rope confinement: Full vs. STrip wrapping for enhanced concrete strength and ductility.” *Case Studies in Construction Materials*, 22: e04134. Elsevier. https://doi.org/10.1016/J.CSCM.2024.E04134.

Saingam, P., Q. Hussain, G. Sua-iam, A. Nawaz, and A. Ejaz. 2024a. “Hemp Fiber-Reinforced Polymers Composite Jacketing Technique for Sustainable and Environment-Friendly Concrete.” *Polymers 2024, Vol. 16, Page 1774*, 16 (13): 1774. Multidisciplinary Digital Publishing Institute. https://doi.org/10.3390/POLYM16131774.

Saingam, P., Q. Hussain, G. Sua-iam, A. Nawaz, and A. Ejaz. 2024b. “Hemp Fiber-Reinforced Polymers Composite Jacketing Technique for Sustainable and Environment-Friendly Concrete.” *Polymers 2024, Vol. 16, Page 1774*, 16 (13): 1774. Multidisciplinary Digital Publishing Institute. https://doi.org/10.3390/POLYM16131774.

Saljoughian, A., and D. Mostofinejad. 2016. “Corner Strip-Batten Technique for FRP-Confinement of Square RC Columns under Eccentric Loading.” *Journal of Composites for Construction*, 20 (3): 04015077. American Society of Civil Engineers (ASCE). https://doi.org/10.1061/(ASCE)CC.1943-5614.0000644/ASSET/C97B1CEC-26AB-4F25-89F5-D36C3F9E9D24/ASSETS/IMAGES/LARGE/FIGURE8.JPG.

Salmaninezhad, M., and S. M. Jazayeri Moghaddas. 2021. “A multi-attribute approach to select the best method for repairing river bridge columns.” *Engineering, Construction and Architectural Management*. Emerald Group Holdings Ltd. https://doi.org/10.1108/ECAM-03-2021-0261/FULL/PDF.

Shaw, I., and B. Andrawes. 2017. “Repair of damaged end regions of PC beams using externally bonded FRP shear reinforcement.” *Construction and Building Materials*, 148: 184–194. Elsevier. https://doi.org/10.1016/J.CONBUILDMAT.2017.05.077.

Song, B., L. Jin, J. Zhang, and X. Du. 2023. “Size effect tests on shear strength of Basalt FRP-RC deep beams with different shear-span ratios.” *Engineering Structures*, 294: 116740. Elsevier. https://doi.org/10.1016/J.ENGSTRUCT.2023.116740.

Tang, Z., W. Li, V. W. Y. Tam, and L. Yan. 2020. “Mechanical performance of CFRP-confined sustainable geopolymeric recycled concrete under axial compression.” *Engineering Structures*, 224: 111246. Elsevier. https://doi.org/10.1016/J.ENGSTRUCT.2020.111246.

Thansirichaisree, P., H. Mohamad, A. Ejaz, P. Saingam, Q. Hussain, and S. Suparp. 2024. “Stress-strain behavior of square concrete columns confined with hybrid B-CSM composites and development of novel prediction models.” *Composites Part C: Open Access*, 14: 100448. Elsevier. https://doi.org/10.1016/J.JCOMC.2024.100448.

Vandoros, K. G., and S. E. Dritsos. 2008. “Concrete Jacket Construction Detail Effectiveness when Strengthening RC Columns.” *Construction and Building Materials*, 22 (3): 264–276. Elsevier. https://doi.org/10.1016/J.CONBUILDMAT.2006.08.019.

Wang, W., M. N. Sheikh, A. Q. Al-Baali, and M. N. S. Hadi. 2018. “Compressive behaviour of partially FRP confined concrete: Experimental observations and assessment of the stress-strain models.” *Construction and Building Materials*, 192: 785–797. Elsevier. https://doi.org/10.1016/J.CONBUILDMAT.2018.10.105.

Yang, K. H., J. H. Mun, M. S. Cho, and T. H. K. Kang. 2014. “Stress-Strain Model for Various Unconfined Concretes in Compression.” *ACI Structural Journal*, 111 (4): 819–826. American Concrete Institute. https://doi.org/10.14359/51686631.

Yooprasertchai, E., A. Bahrami, P. Saingam, Q. Hussain, A. Ejaz, and P. Joyklad. 2023a. “Incorporation of Steel Fibers to Enhance Performance of Sustainable Concrete Made with Waste Brick Aggregates: Experimental and Regression-Based Approaches.” *Buildings 2023, Vol. 13, Page 2820*, 13 (11): 2820. Multidisciplinary Digital Publishing Institute. https://doi.org/10.3390/BUILDINGS13112820.

Yooprasertchai, E., A. Ejaz, P. Saingam, A. W. M. Ng, and P. Joyklad. 2023b. “Development of Stress-Strain Models for Concrete Columns Externally Strengthened with Steel Clamps.” *Construction and Building Materials*, 377: 131155. Elsevier. https://doi.org/10.1016/J.CONBUILDMAT.2023.131155.

Zeng, J. J., Y. C. Guo, W. Y. Gao, J. Z. Li, and J. H. Xie. 2017. “Behavior of Partially and Fully FRP-Confined Circularized Square Columns under Axial Compression.” *Construction and Building Materials*, 152: 319–332. Elsevier. https://doi.org/10.1016/J.CONBUILDMAT.2017.06.152.